P CYGNI TYPE PROFILES

A. Peraiah and M. Srinivasa Rao

Abstract

We have presented a series of P Cygni type profiles of spectral lines computed by employing different velocity laws of expansion in a spherically symmetric atmosphere. A comparison has been made with those of Beals classification. In many cases we have calculated the profiles by changing the density and velocity according to the equation of conservation of mass viz., $4\pi r^2 \rho v$ = constant where ρ and v are the density and velocity at the radial point r respectively. We have employed the line transfer equation in comoving frame in certain test cases, to obtain the source function which is being used to calculate the profiles observed at infinity. However, this procedure is relaxed in many cases as it becomes time consuming and we have employed a source function which is a function of either the radius or the number of a given shell from the centre of the star.

Key words: P Cygni type profiles, source function, radiative transfer.

Introduction

It is well know that the lines in the spectrum of P Cygni show peculiar characteristics in that there is emission on the redside and absorption on the blue side. Beals (1950) has classified all these profiles into 7 or 8 classes although many more variations are noted in the spectra of such stars. It is difficult to simulate these spectra theoretically as the problems of solving the line transfer are formidable. It is only in the recent past that we understood how to tackle these problems with most of the physical proceses of line formation taken into account. The problem is still far from total comprehension. We should know first of all the radiation field and the nature of bulk motion and the interaction between these two. We have to simulate the line profiles observed in expanding shells, by assuming a velocity law that operates in the expanding spherical shells. We calculated several P Cygni type profiles and presented in the next section.

2. Description of the Results

In Figure (1a) we have reproduced the Beals classification and in Figure (1b) we give a schematic diagram of the geometry of the line forming region of the atmosphere. The region S is the star and the region X,X' Z and Y are the part of the atmosphere. This is divided into several concentric spherical shells. The region Y is occulted by the stars disc and therefore no radiation

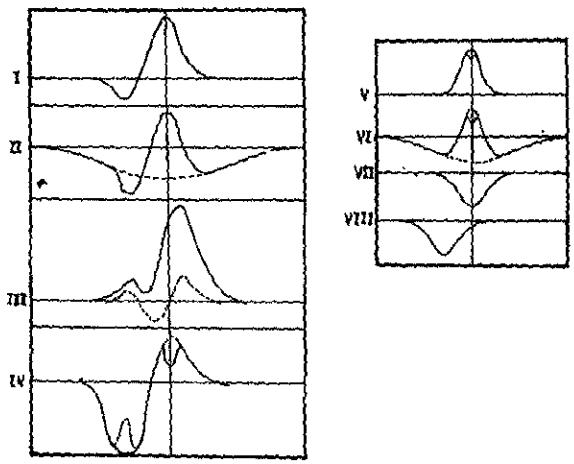

Fig.1 (a) Beals classification of P cygni type profiles.

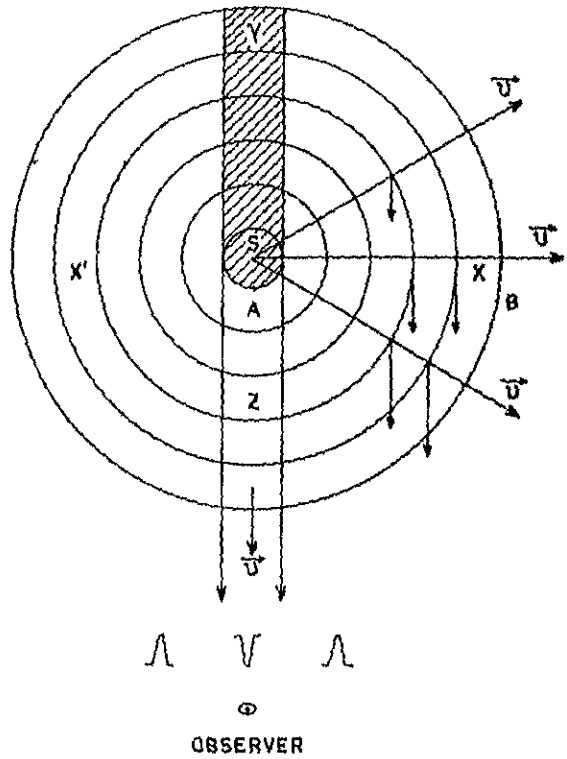

Fig.1 (b) Schematic diagram of the geometry of line forming region.

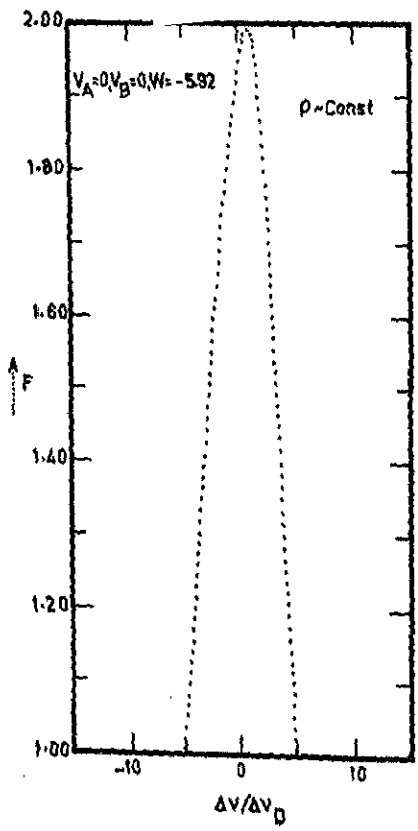

Fig.2 Line profiles with $S \sim r^{-1}$; $\tau = 12.50$

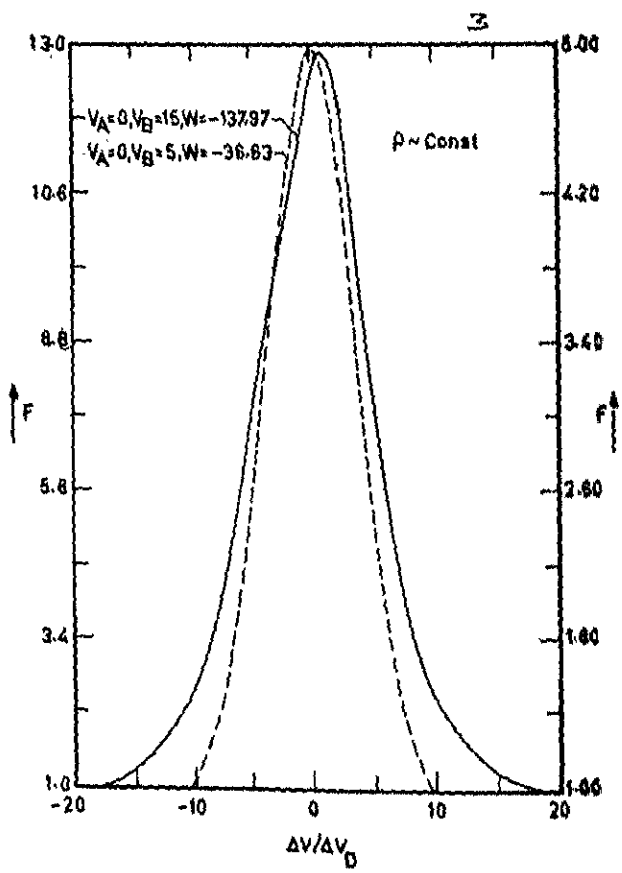

Fig.3 Line profiles with $S \sim r^{-1}$; $\tau = 12.50$

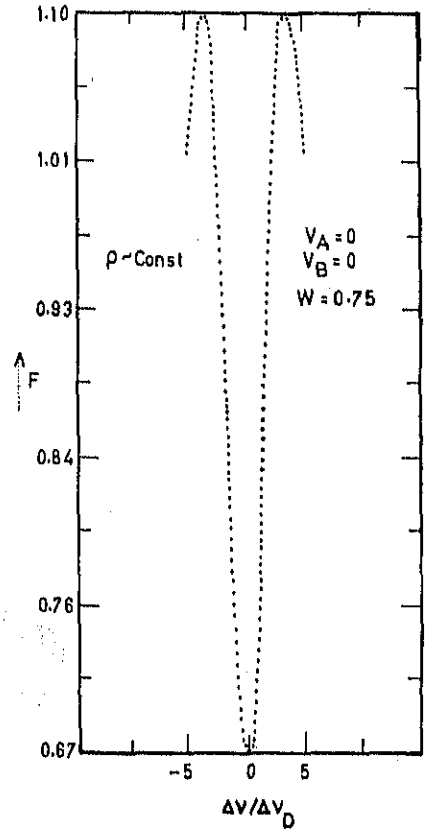

Fig.4 Line profiles with $S \sim \frac{1}{r^2}$; τ = 12.50

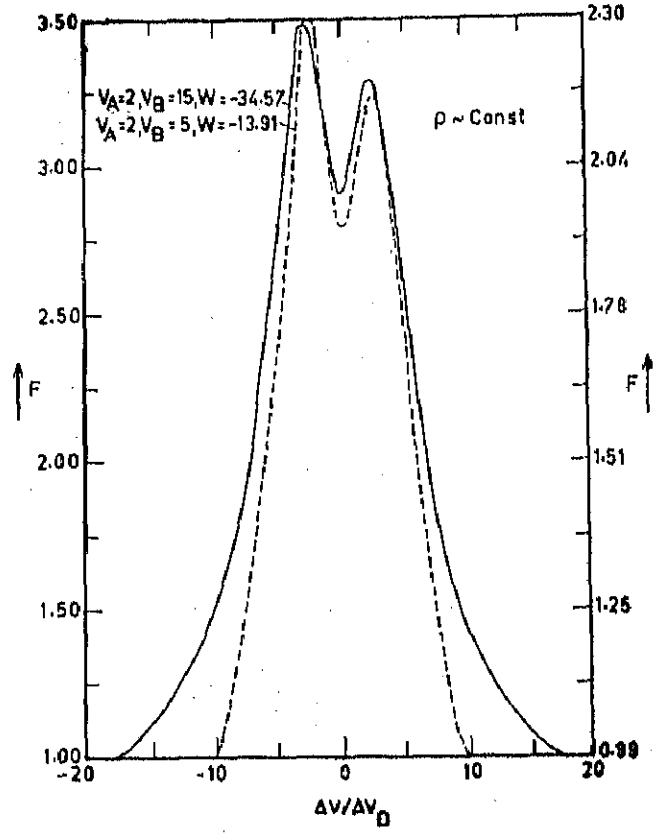

Fig.5 Line profiles with $S \sim \frac{1}{r^2}$; τ = 12.50

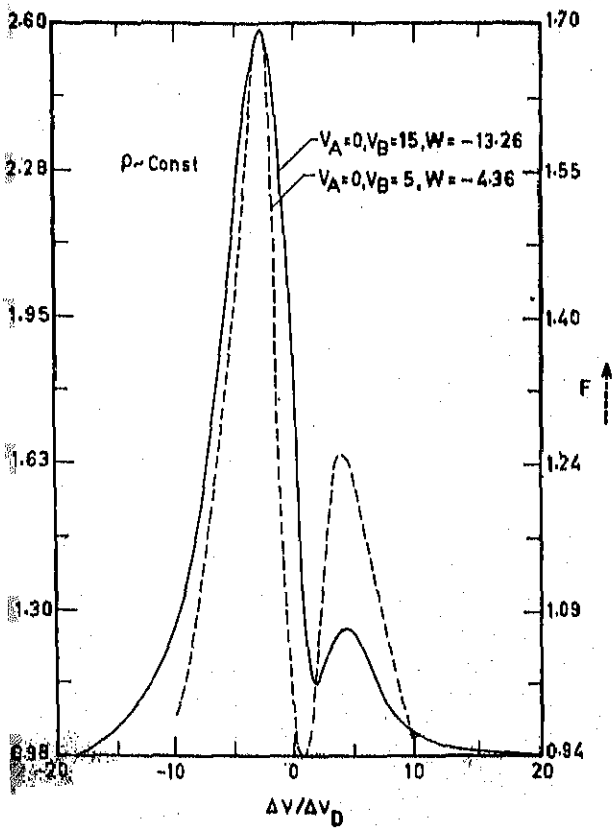

Fig.6 Line profiles with $S \sim \frac{1}{r^2}$; τ = 12.50

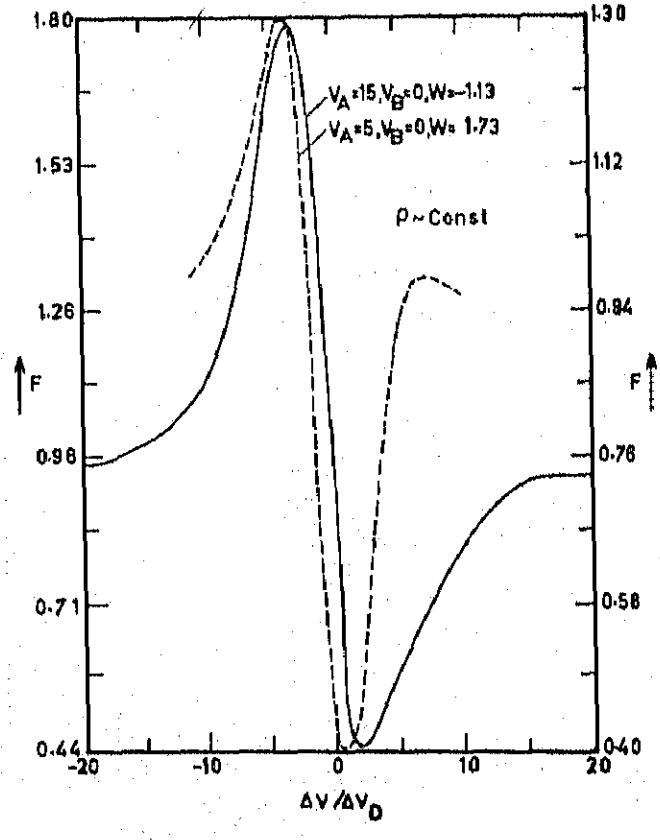

Fig.7 Line profiles with $S \sim \frac{1}{r^2}$; τ = 12.50

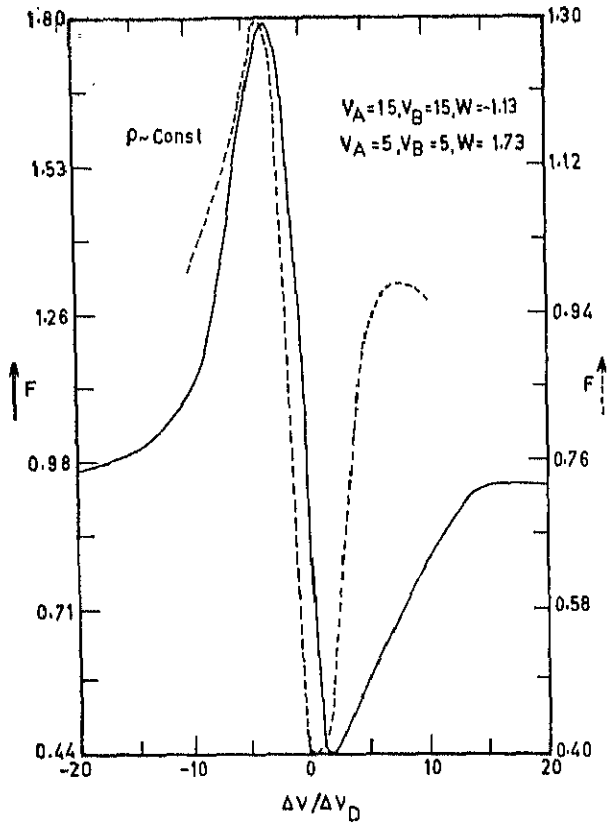

Fig.8 Line profiles with $S \sim \frac{1}{r^3}$; τ = 12.50

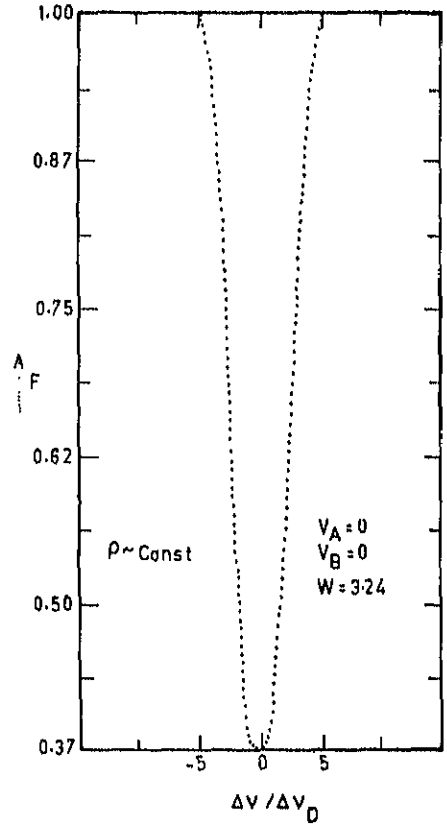

Fig.9 Line profiles with $S \sim \frac{1}{n}$; τ = 12.50

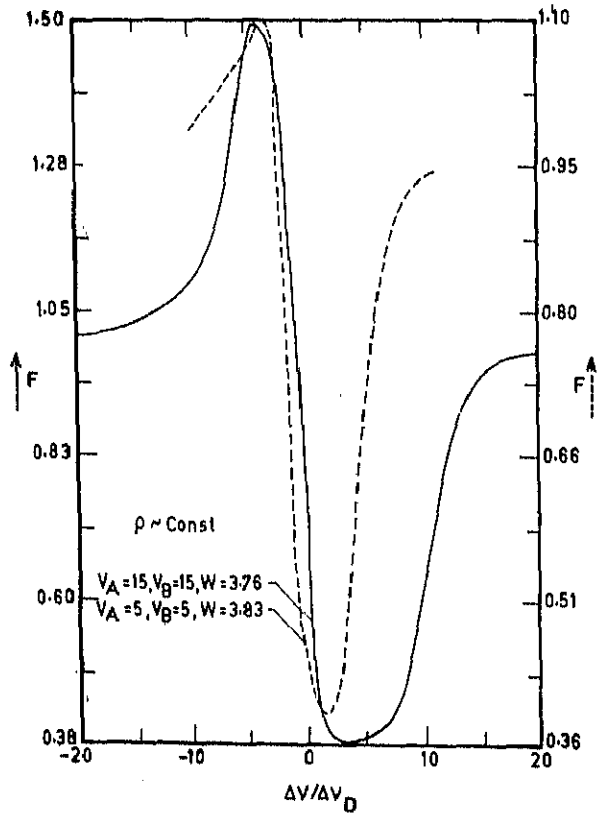

Fig.10 Line profiles with $S \sim \frac{1}{n}$; τ = 12.50

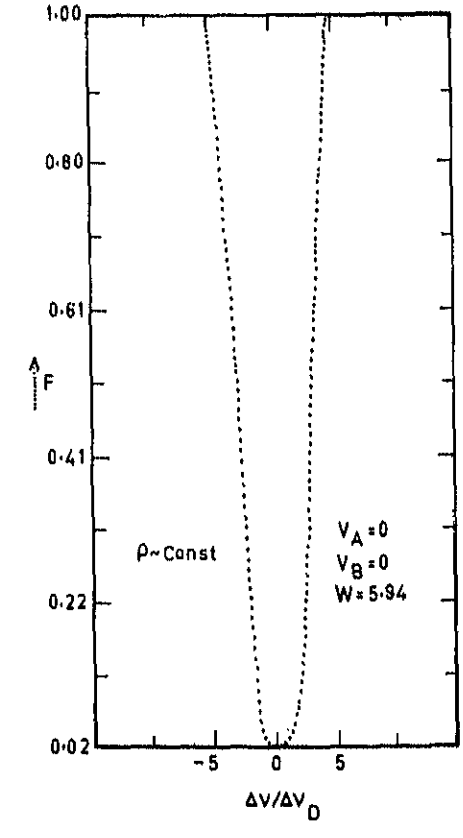

Fig.11 Line profiles with $S \sim \frac{1}{n^2}$; τ = 12.50

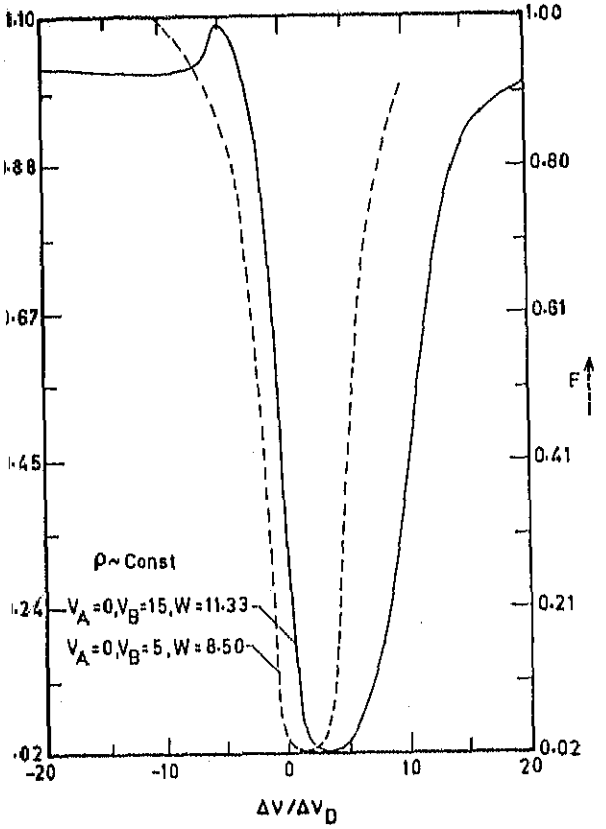

Fig.12 Line profiles with $S \sim \frac{1}{n^2}$; τ = 12.50

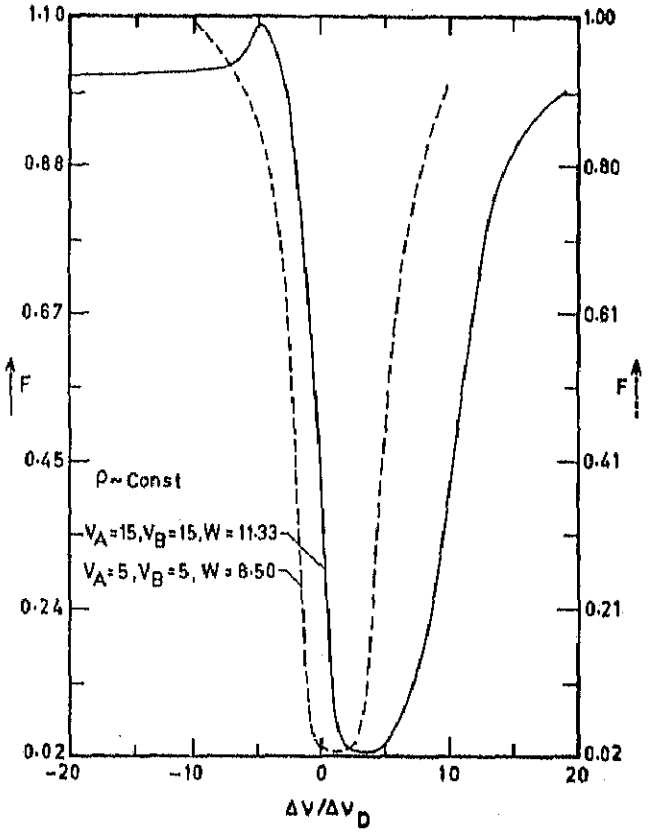

Fig.13 Line profiles with $S \sim \frac{1}{n^2}$; τ = 12.50

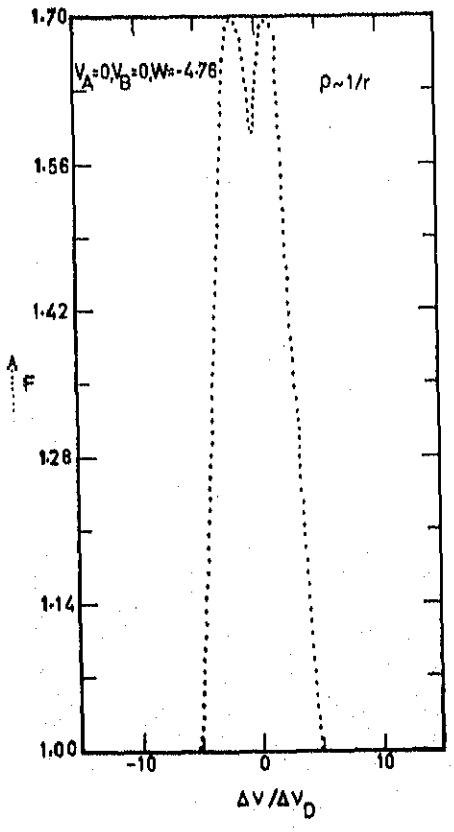

Fig.14 Line profiles with $S \sim \frac{1}{r}$; τ = 7.007

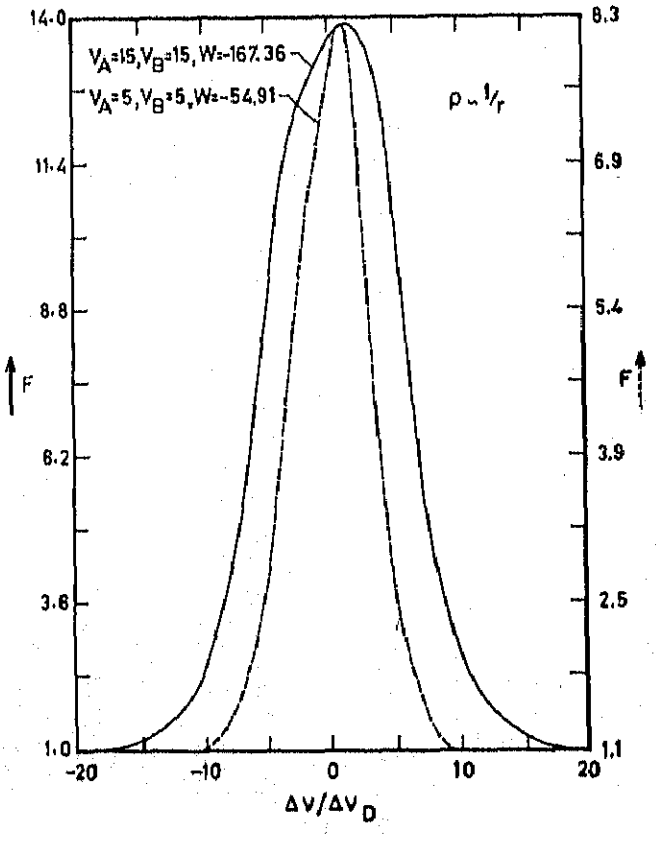

Fig.15 Line profiles with S ~ r ; τ = 7.007

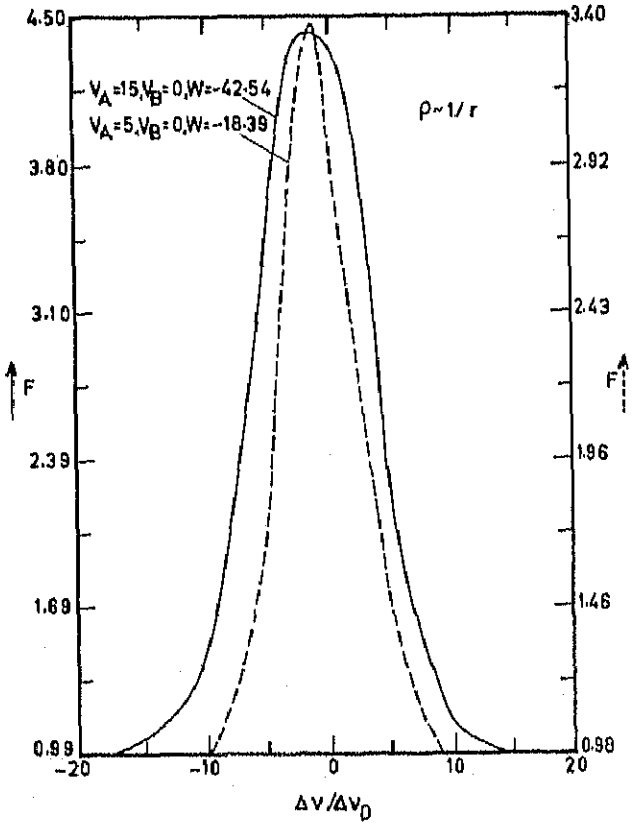

Fig.16 Line profiles with $S \sim \frac{1}{r}$; τ = 7.007

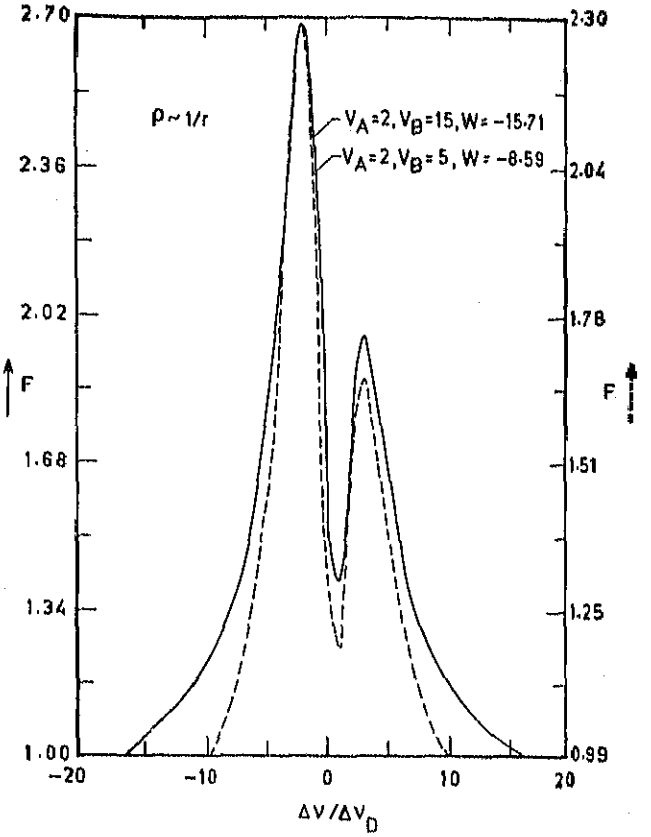

Fig.17 Line profiles with $S \sim \frac{1}{r}$; τ = 7.007

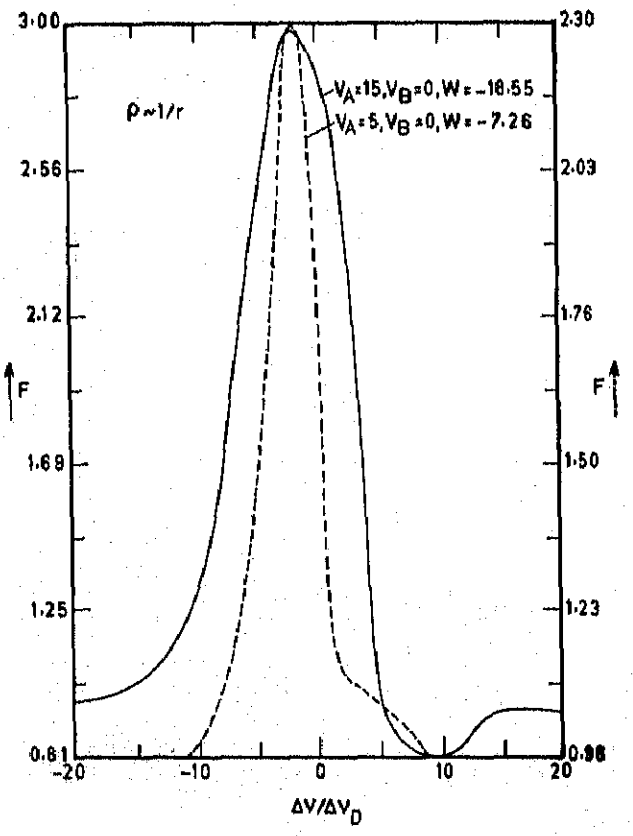

Fig.18 Line profiles with $S \sim \frac{1}{r^2}$; τ = 7.007

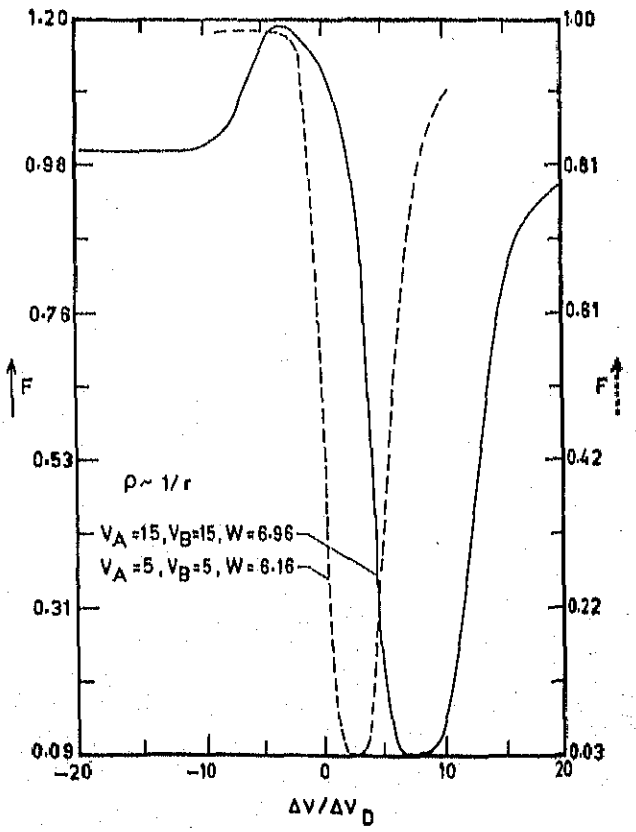

Fig.19 Line profiles with $S \sim \frac{1}{n^2}$; τ = 7.007

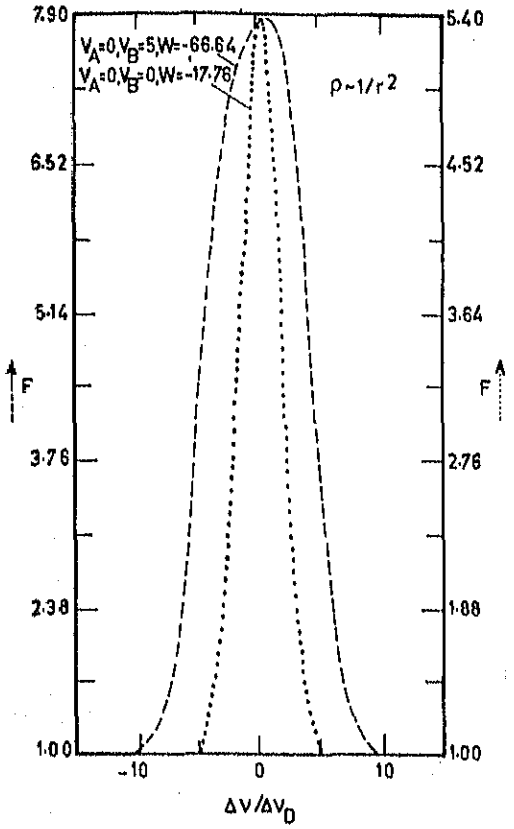

Fig.20 Line profiles with $S \sim r$; $\tau = 4.356$

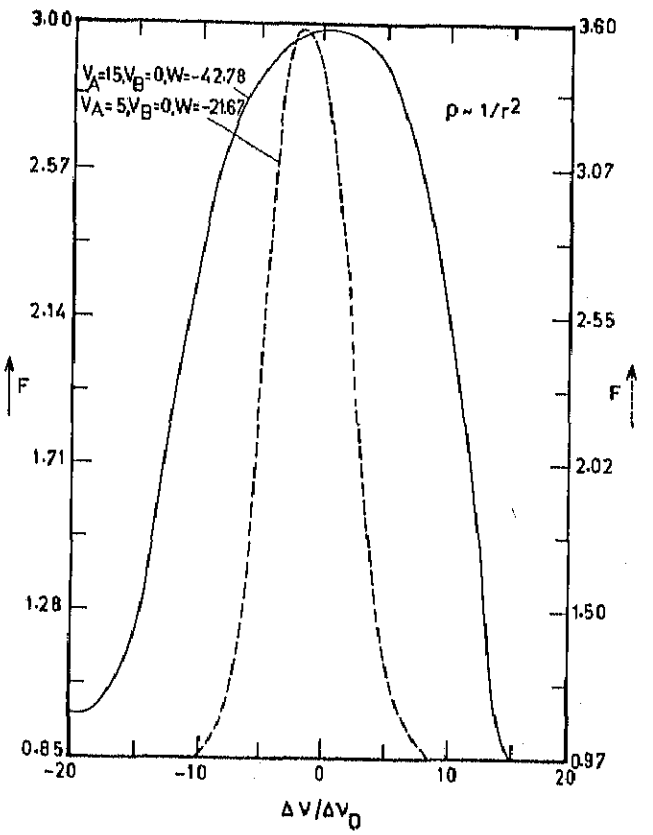

Fig.21 Line profiles with $S \sim \frac{1}{r}$; $\tau = 4.356$

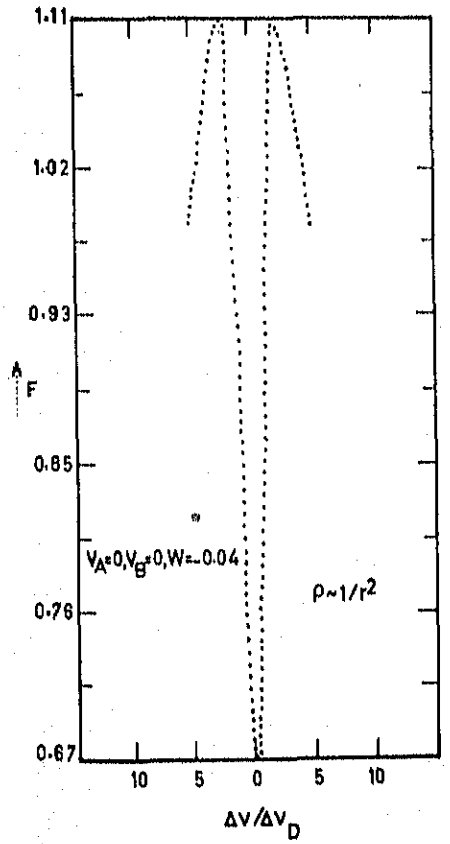

Fig.22 Line profiles with $S \sim \frac{1}{r^3}$; $\tau = 4.356$

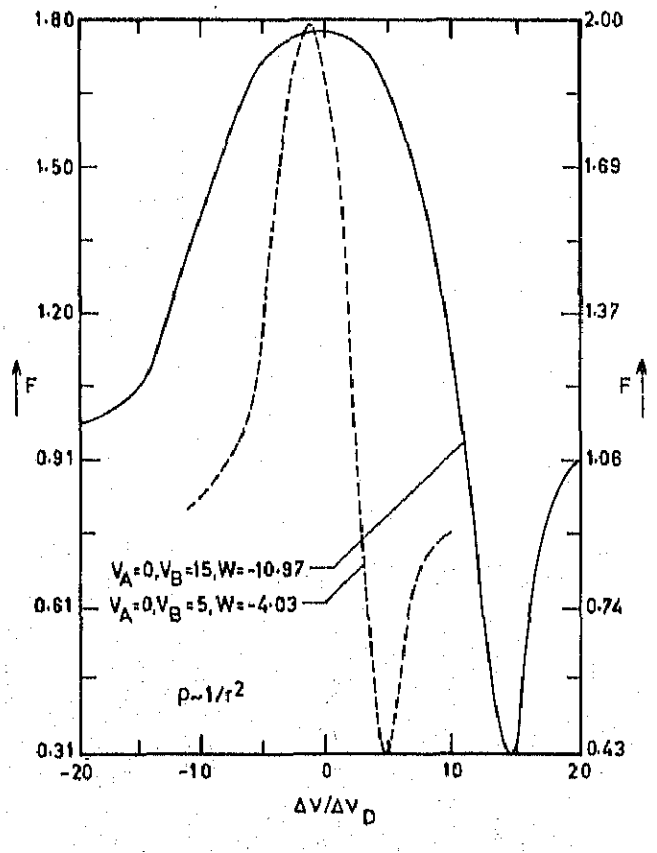

Fig.23 Line profiles with $S \sim \frac{1}{r^3}$; $\tau = 4.356$

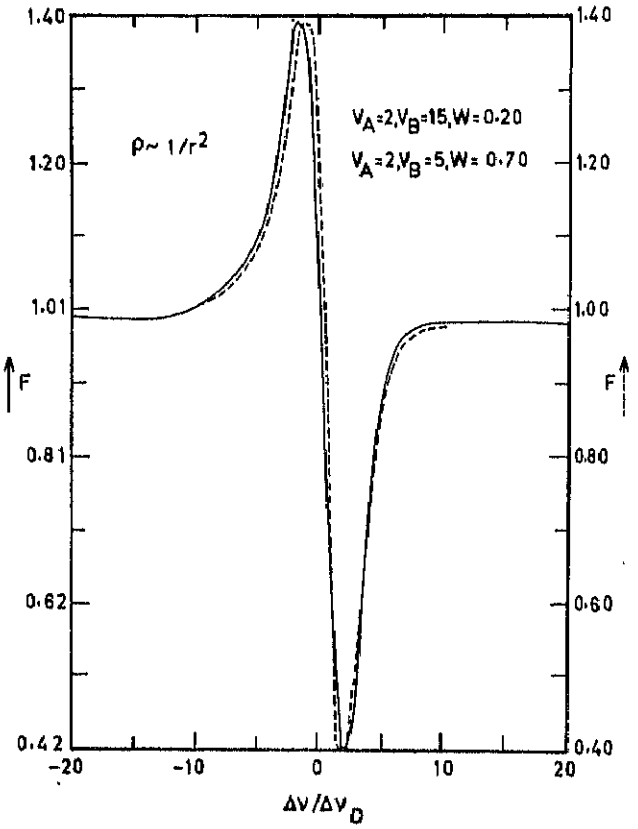

Fig.24 Line profiles with $S \sim \frac{1}{n}$; τ = 4.356

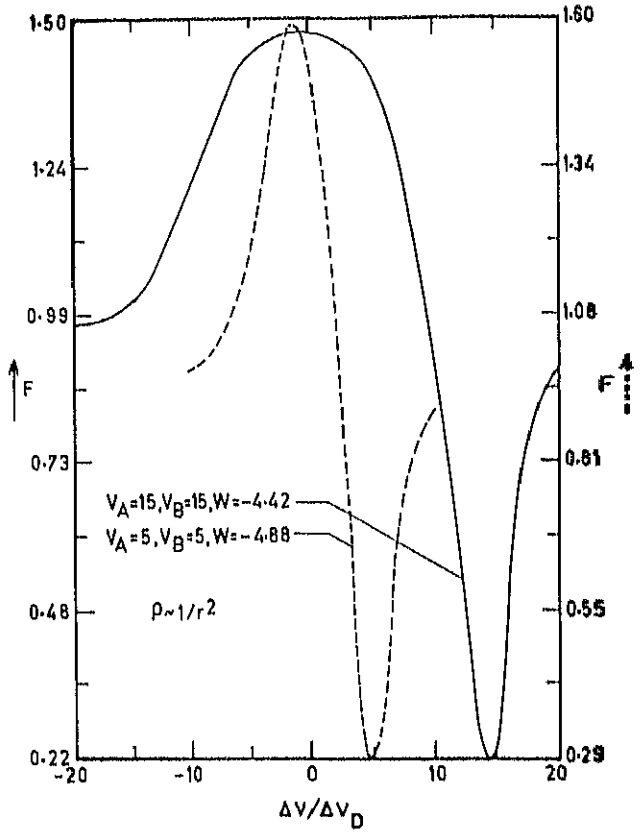

Fig.25 Line profiles with $S \sim \frac{1}{n}$; τ = 4.356

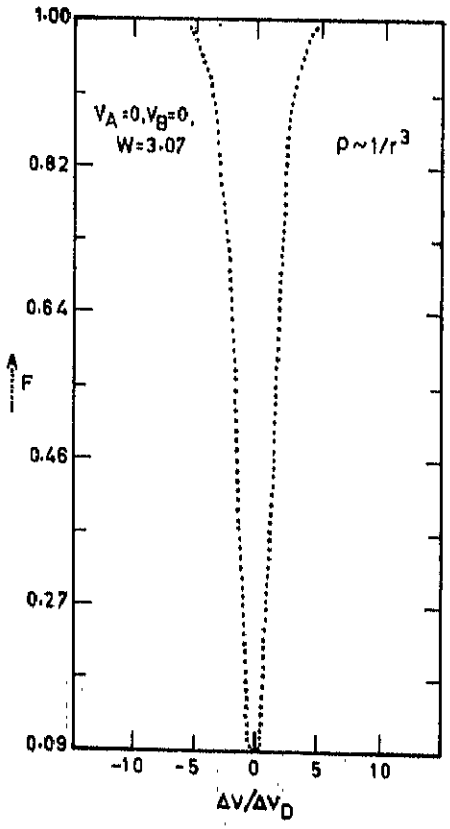

Fig.26 Line profiles with $S \sim \frac{1}{n^3}$; τ = 2.985

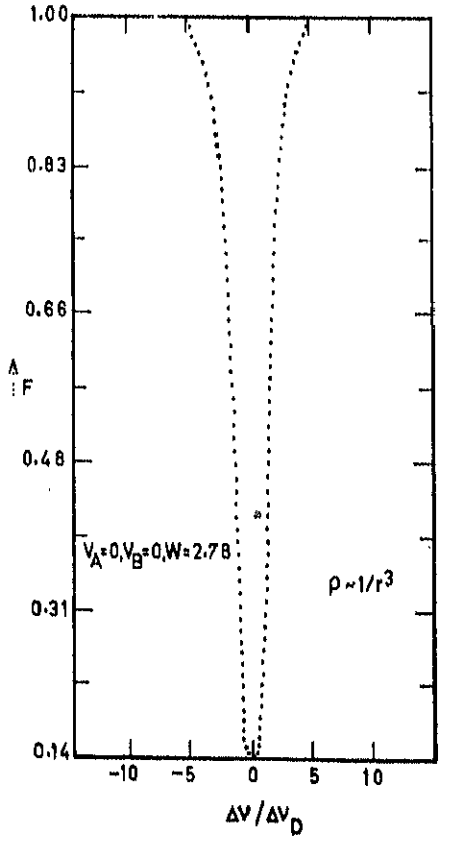

Fig.27 Line profiles with $S \sim \frac{1}{n^2}$; τ = 2.985

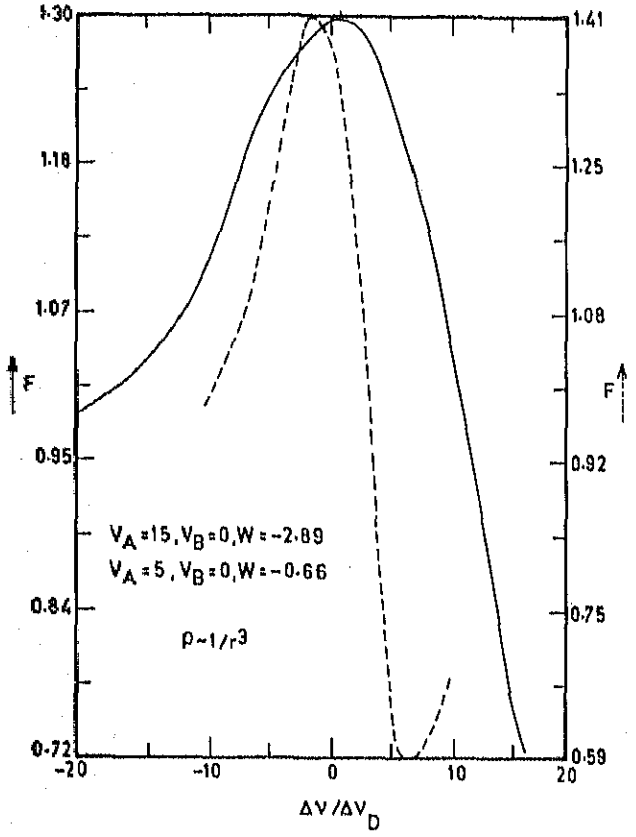

Fig.28 Line profiles with $S \sim \frac{1}{n}$; τ = 2.985

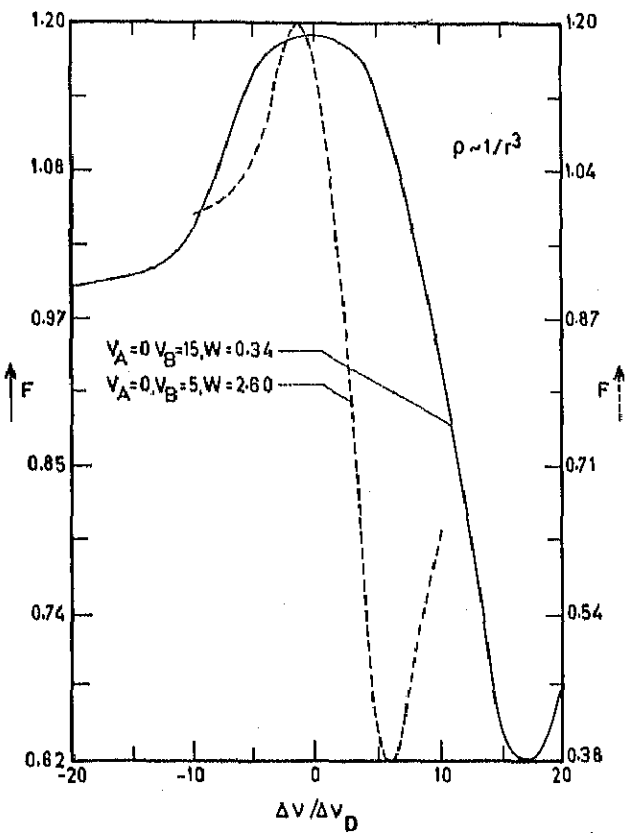

Fig.29 Line profiles with $S \sim \frac{1}{n^2}$; τ = 2.985

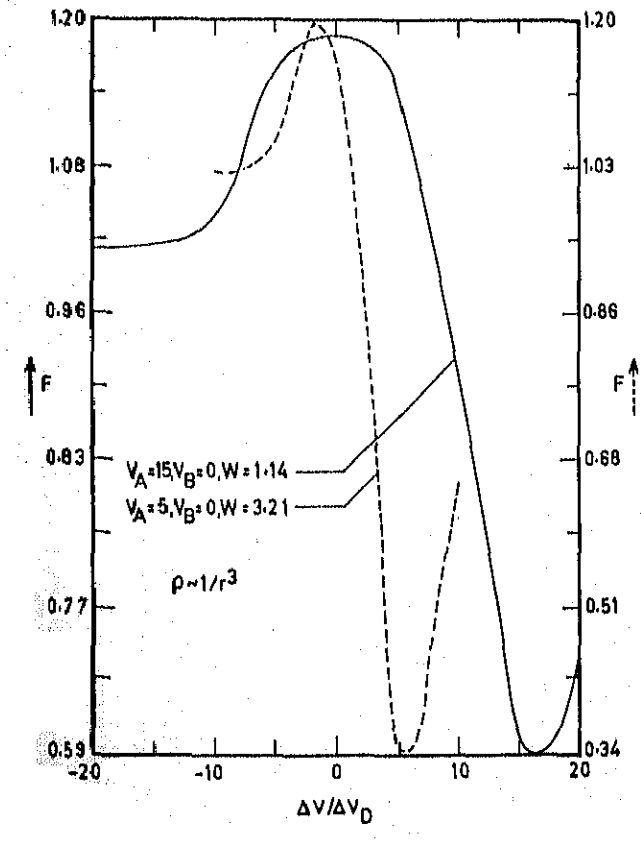

Fig.30 Line profiles with $S \sim \frac{1}{n^3}$; τ = 2.985

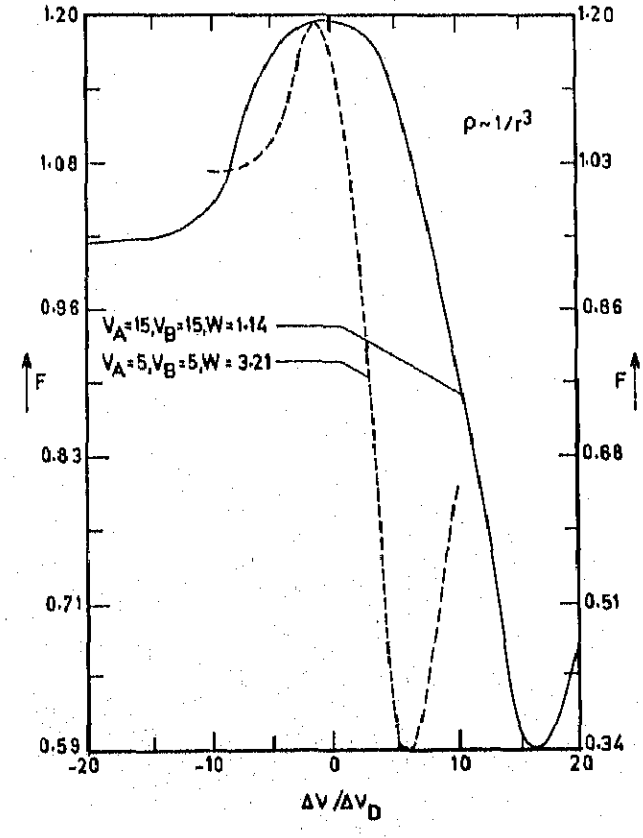

Fig.31 Line profiles with $S \sim \frac{1}{n^3}$; τ = 2.985

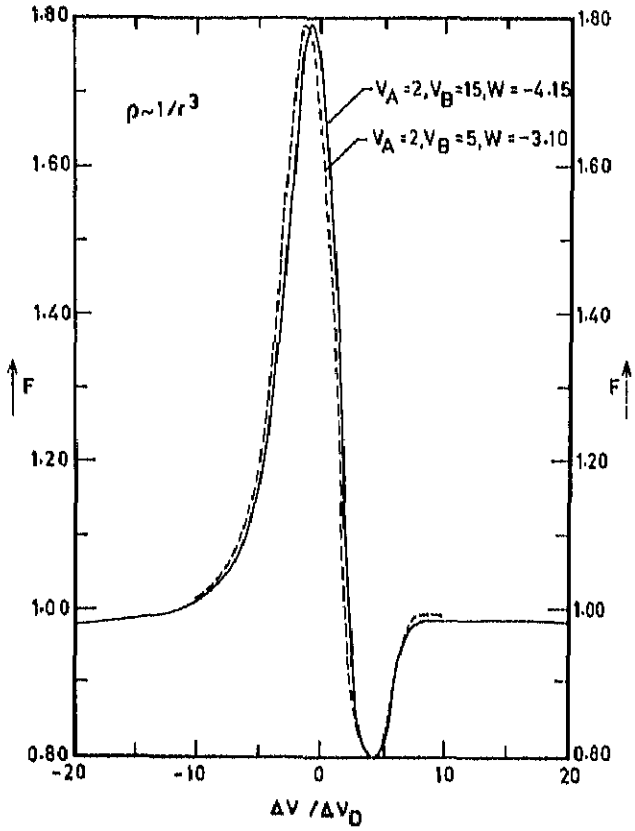

Fig.32 Line profiles with $S \sim \frac{1}{n^3}$; τ = 2.985

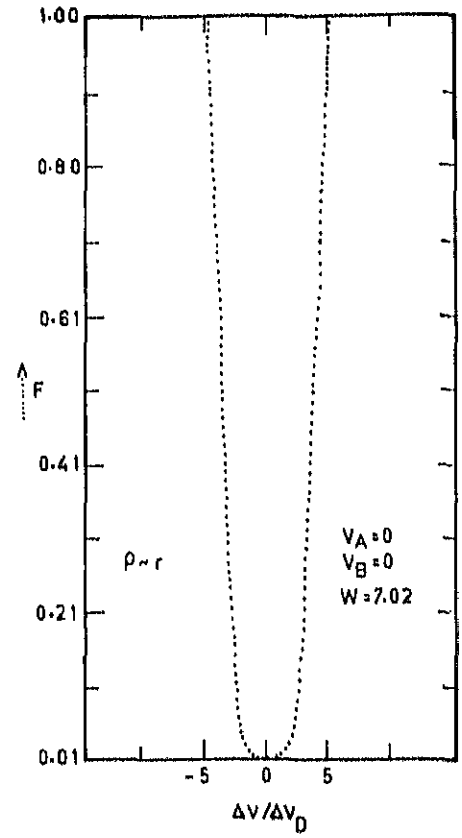

Fig.33 Line profiles with $S \sim \frac{1}{n^2}$; τ = 24.583

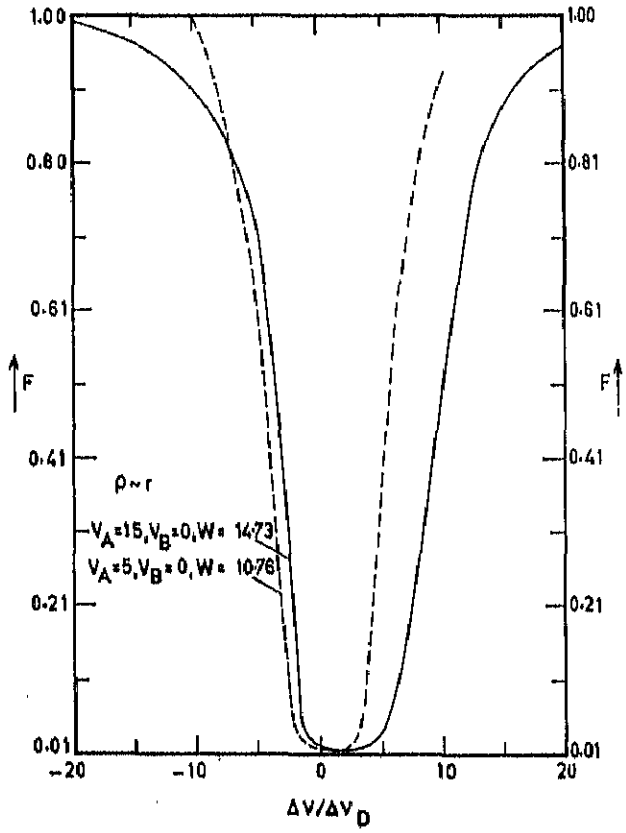

Fig.34 Line profiles with $S \sim \frac{1}{n^2}$; τ = 24.583

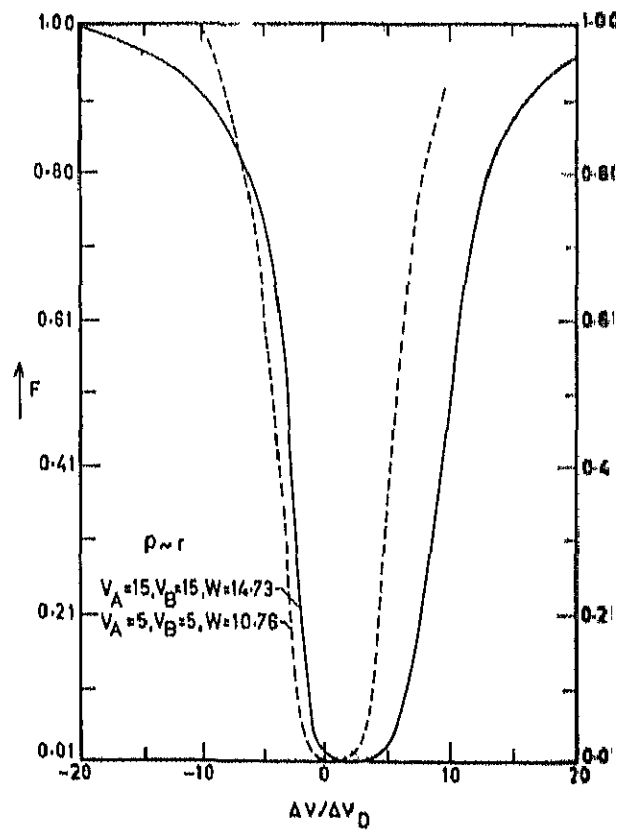

Fig.35 Line profiles with $S \sim \frac{1}{n^2}$; τ = 24.583

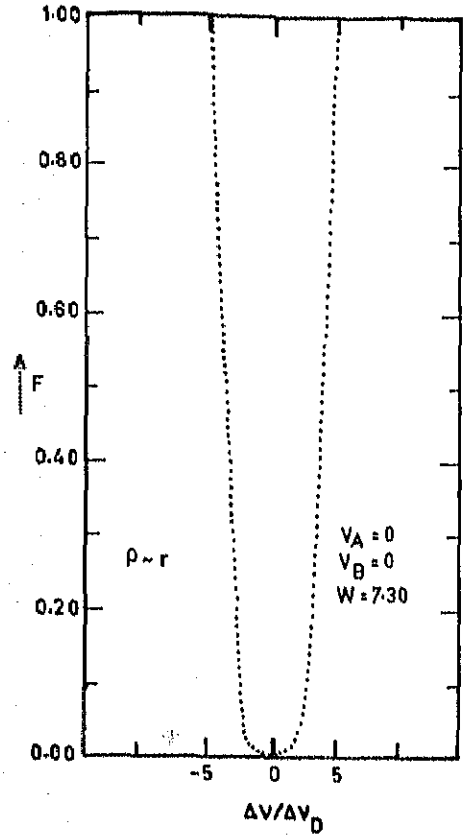

Fig.36 Line profiles with $S \sim \frac{1}{n^3}$; τ = 24.583

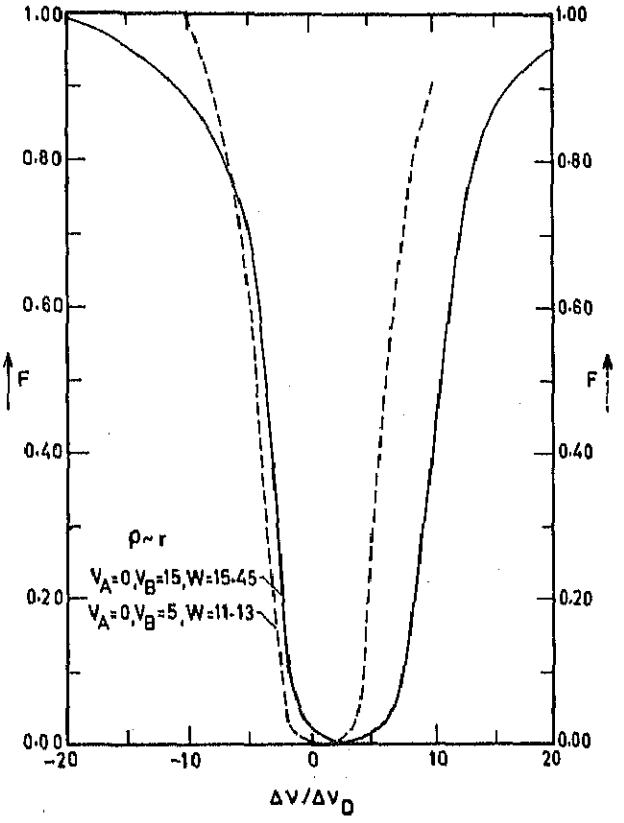

Fig.37 Line profiles with $S \sim \frac{1}{n^3}$; τ = 24.583

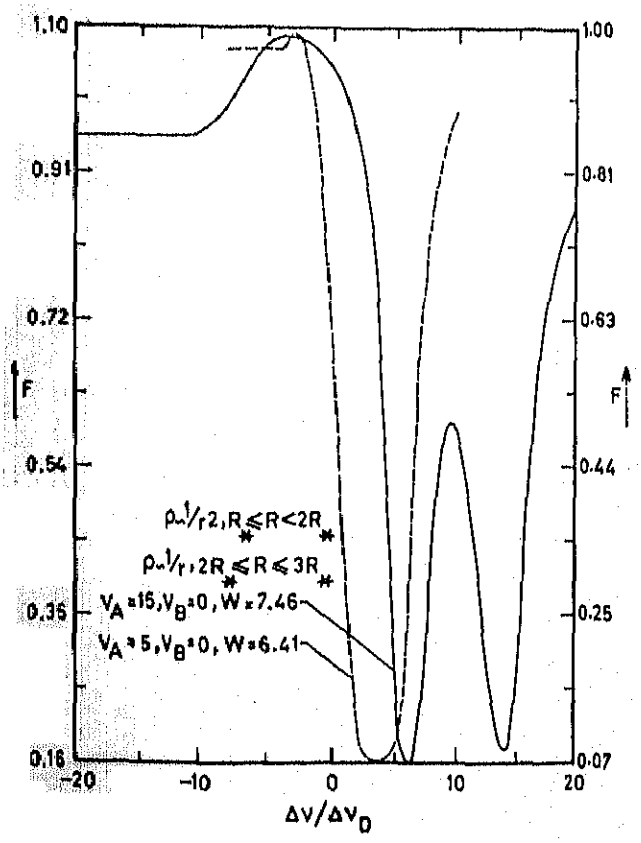

Fig.38 Line profiles with $S \sim \frac{1}{n^3}$; τ = 5.75

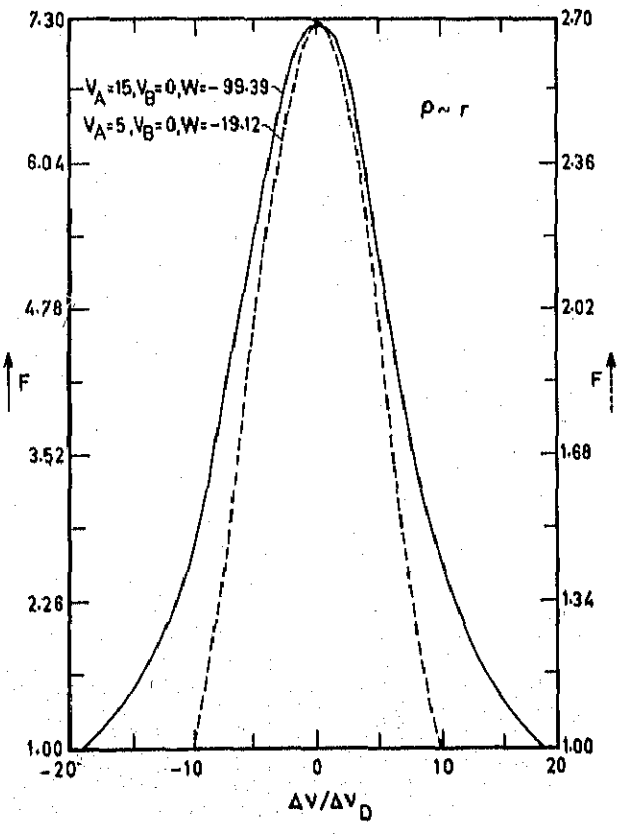

Fig.39 Line profiles with $S \sim r$; τ = 24.583

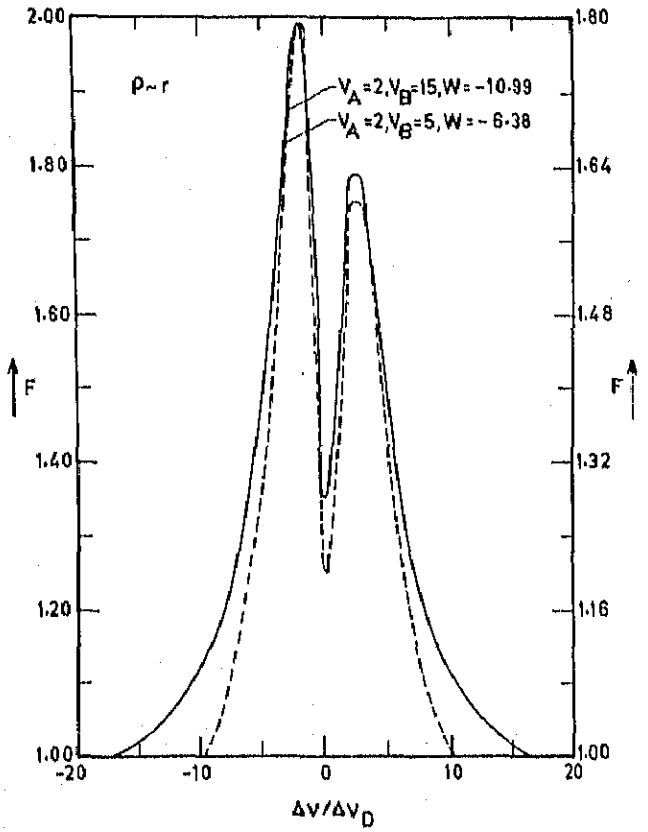

Fig.40 Line profiles with $S \sim \frac{1}{r^2}$; τ = 7.007

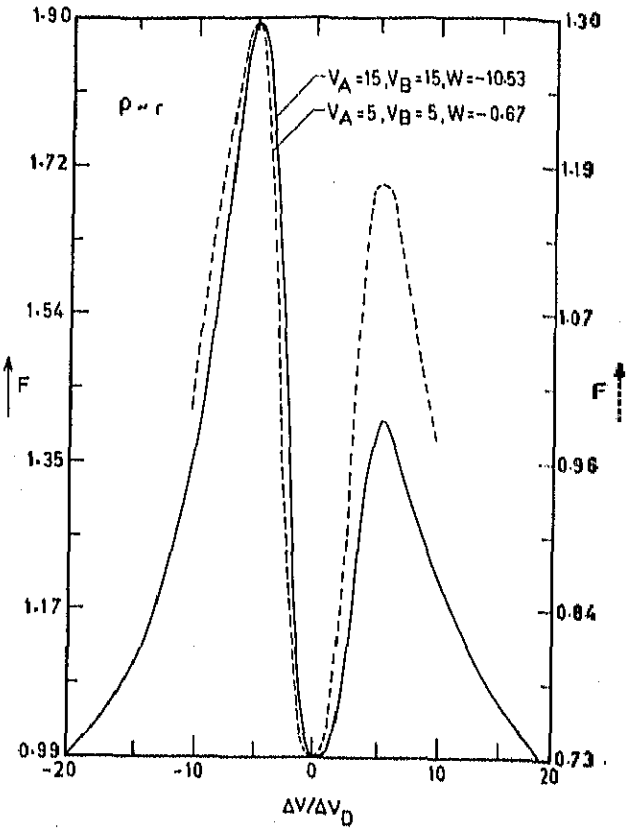

Fig.41 Line profiles with $S \sim \frac{1}{r^2}$; τ = 24.033

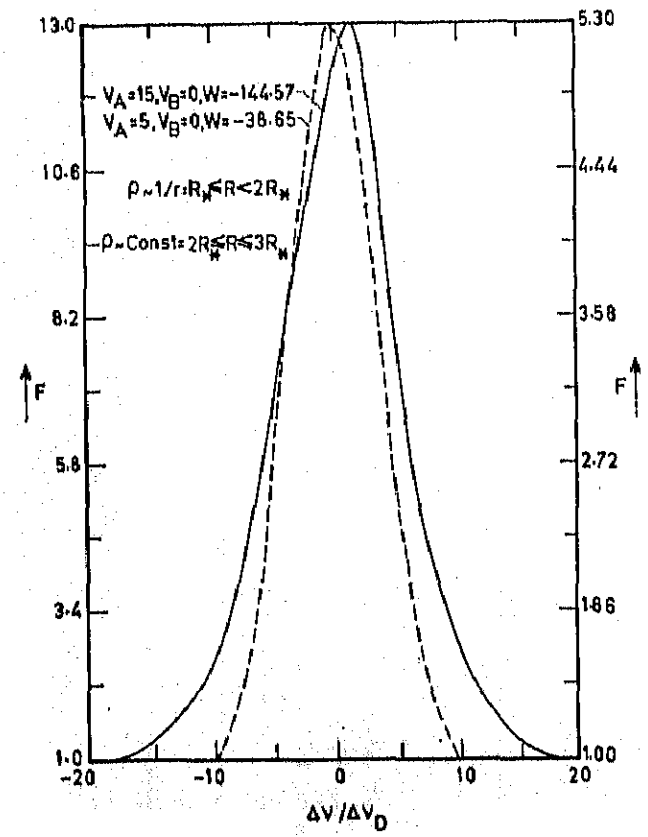

Fig.42 Line profiles with $S \sim r$; τ = 10.480

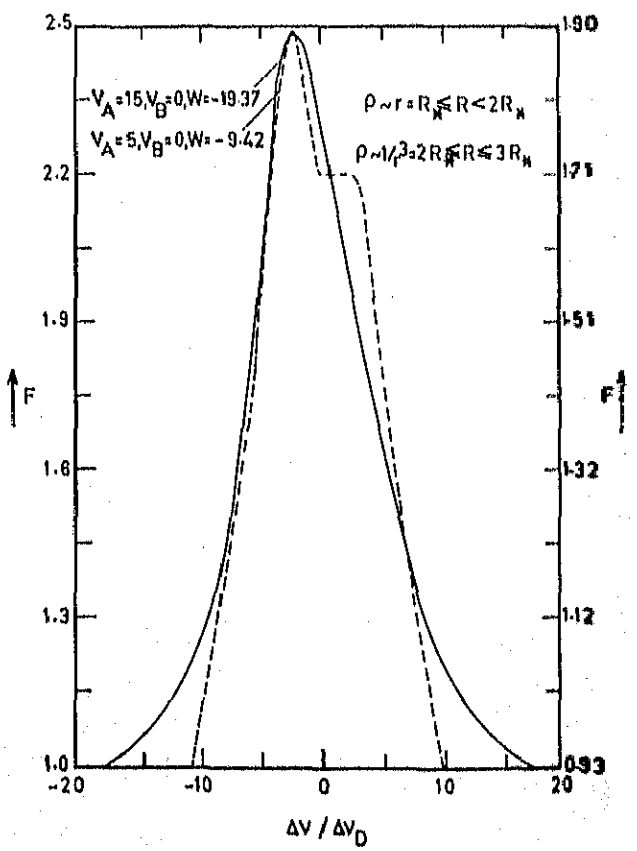

Fig.43 Line profiles with $S \sim \frac{1}{r}$; τ = 10.401

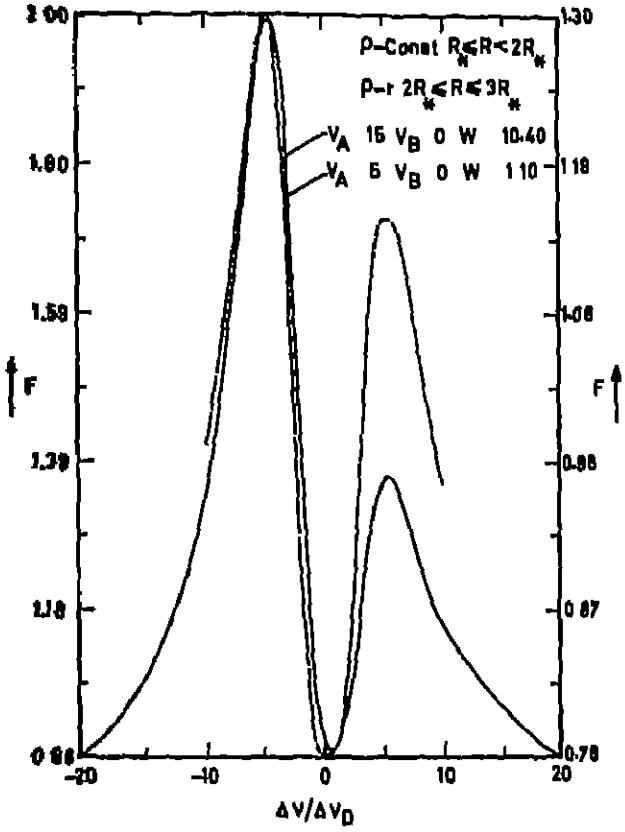

Fig 44 Line profiles with $S \sim \frac{1}{r^2}$; T 21 250

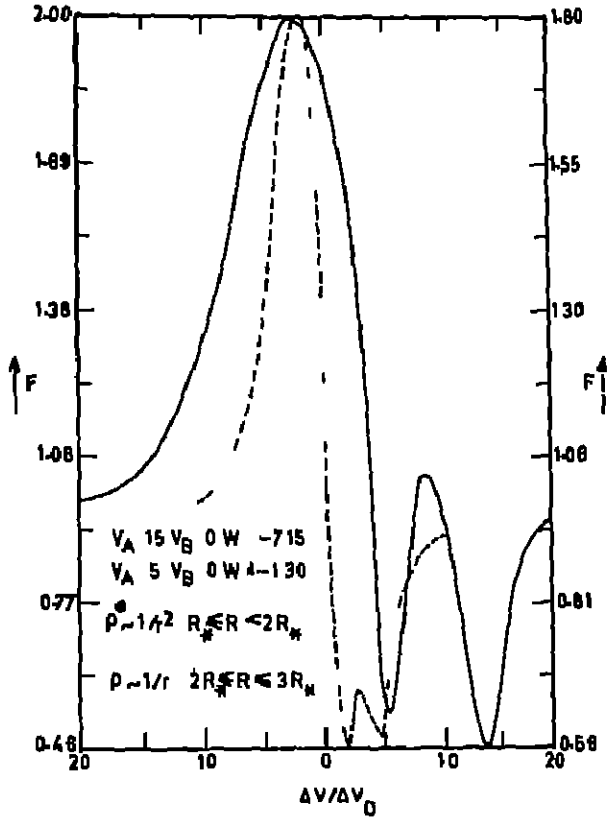

Fig 45 Line profiles with $S \sim \frac{1}{r^3}$; T 5.750

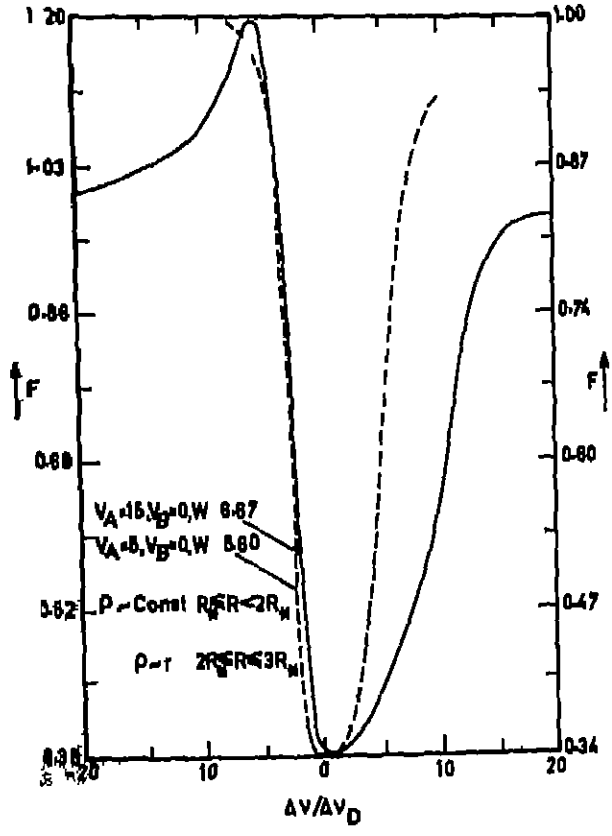

Fig 46 Line profiles with $S \sim \frac{1}{n}$; T 21.250

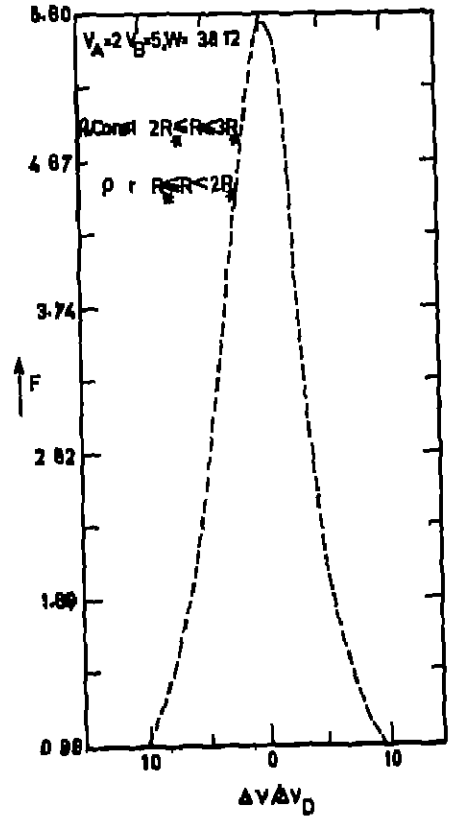

Fig 47 Line profiles with $S \sim \frac{1}{r}$, $R_s \leq R < 2R_s$;

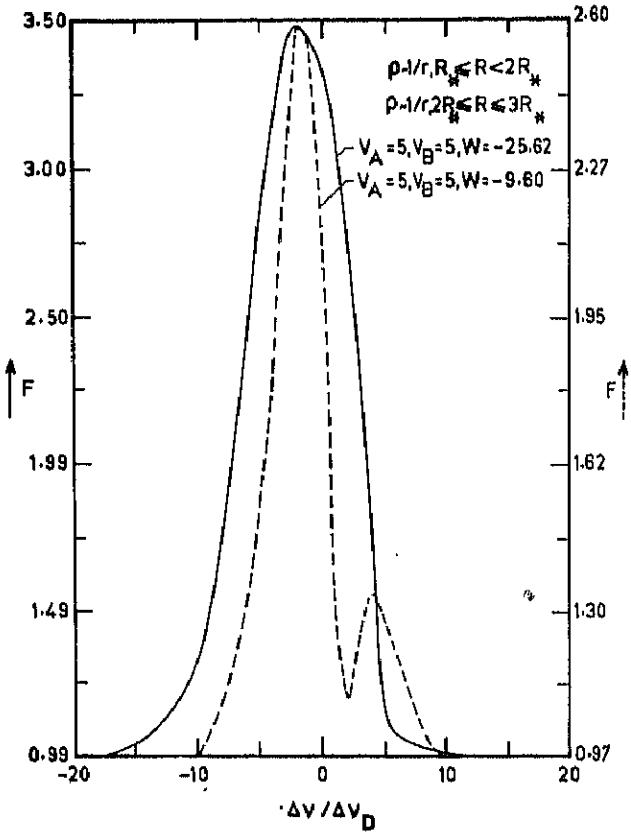

Fig.48 Line profiles with $S \sim \frac{1}{r^3}$, $R_* \leq R < 2R_*$; $S \sim r$, $2R_* \leq R < 3R_*$; $\tau = 15.833$

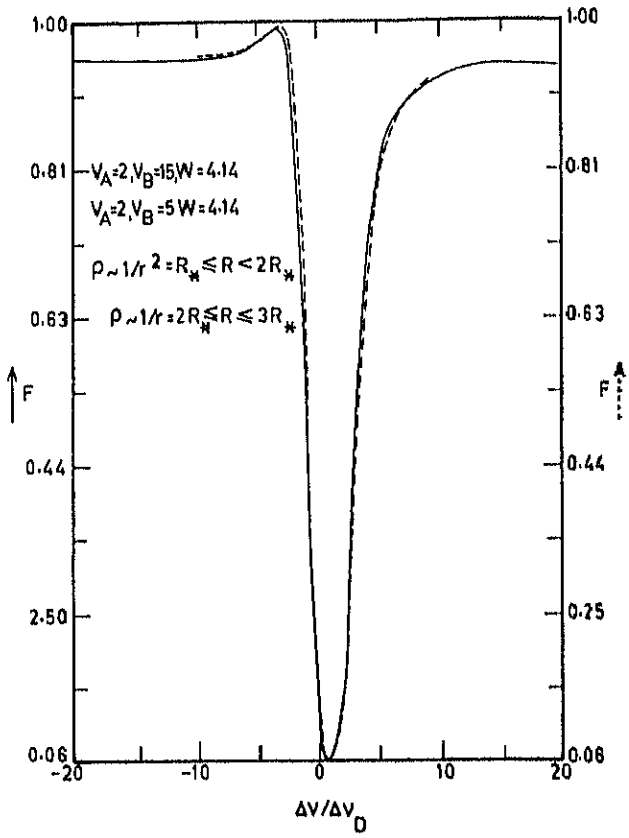

Fig.49 Line profiles with $S \sim \frac{1}{n}$, $R_* \leq R < 2R_*$; $S \sim \frac{1}{n^2}$, $2R_* \leq R < 3R_*$; $\tau = 5.750$

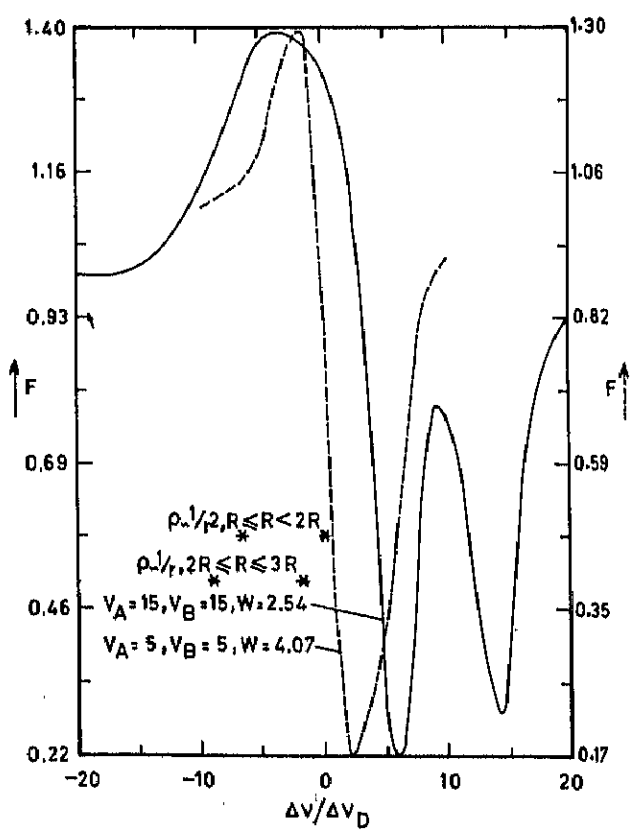

Fig.50 Line profiles with $S \sim \frac{1}{n}$, $R_* \leq R < 2R_*$;

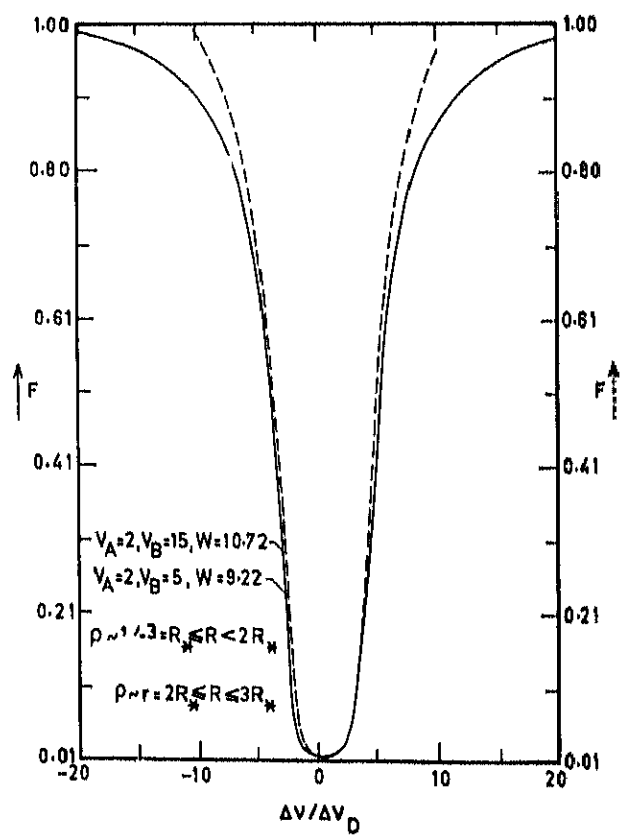

Fig.51 Line profiles with $S \sim \frac{1}{n}$, $R_* \leq R < 2R_*$;

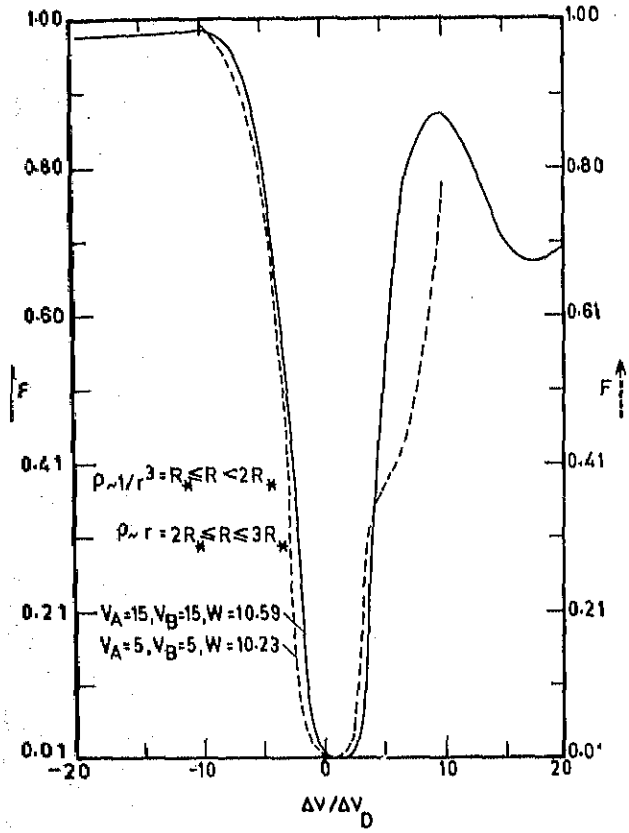

Fig.52 Line profiles with $S \sim \frac{1}{n}$, $R_* \leq R < 2R_*$; $S \sim \frac{1}{n^2}$, $2R_* \leq R < 3R_*$; $\tau = 17.168$

from this region reaches the observer. The matter is flowing out radially as shown in regions X, X' and Z with velocities v. We obtain absorption profiles from the region Z and emission from the regions X and X' as shown in Figure (1b). The specific intensities are calculated along the line of sight as shown in the Figure (1b), by using the formula (Peraiah 1980)

$$I(T) = I_0 \exp(-T) + \int_0^T S(t) \exp[-(T-t)]\, dt \quad (1)$$

where S(t) is the source function, T is the total optical depth in the shell along the ray path, I is the specific intensity. The density and velocity law are governed by the relation

$$4\pi r^2 \rho v = \text{constant} \quad (2)$$

The atmosphere is divided into 100 shells with the following data.

$$\begin{aligned} \text{Ne (A)} &= 10^3 \text{ cm}^{-3} \\ \text{B/A} &= 3 \\ R_{in} &= 10^{12} \text{ cm} \\ R_{out} &= 3 \times 10^{12} \text{ cm} \end{aligned} \quad (3)$$

The optical depth is given by

$$\Delta\tau = \sigma \text{ Ne } (r) \quad \Delta r \quad (4)$$

where Ne (r) is the electron density at r and σ is the Thomson scattering coefficient.

We have employed Doppler profile function and all the velocities are defined in terms of Doppler units. The figures are self explanatory and W is the equivalent width given by the formula

$$W = \int_{-\infty}^{+\infty} \left(1 - \frac{F_\nu}{F_c}\right) d\nu \quad (5)$$

where F_ν and F_c are the fluxes at frequency ν and in the continuum. The source function variation and the optical depth calculated by using the equation (4) are given in the figures. V_A and V_B are the velocities at A and B (see Figure 1b) in Doppler units.

References

Beals, C.S., 1950, Pub. Dom. astrophys. Obs. 9, No.1.

Peraiah, A., 1980, J. Astrophys. Astr. 1, 17.